AIAA-98-4308

Autonomous LEO Orbit Determination From Magnetometer and Sun Sensor Data

Mark L. Psiaki*
Cornell University, Ithaca, N.Y. 14853-7501

Abstract

A batch filter has been designed to autonomously estimate the orbit of a LEO spacecraft using data only from a magnetometer and a sun sensor. The goal of this study has been to prove the feasibility of a proposed low-cost, moderate-accuracy autonomous orbit determination system. The system uses a batch filter to estimate the Keplerian orbital parameters, a drag parameter, magnetometer biases, and corrections to the Earth's magnetic field. It does this by minimizing the square errors between measured and estimated values of two quantities, the Earth's magnetic field magnitude and the cosine of the angle between the sun vector and the Earth's magnetic field vector, both measured at the spacecraft. The proposed system is observable, and reasonable accuracy is obtainable. Given a magnetometer with a 10 nT 1-σ accuracy and a sun sensor with a 0.005^{o} 1-σ accuracy, the system can achieve 1-σ position accuracies on the order of 500 m for inclined LEO orbits.

Introduction

Knowledge of orbit and position is a requirement of virtually all spacecraft missions. There exist many orbit determination systems. Traditional systems rely on ground-based range and range-rate data to observe the orbit and position, as in Ref. 1. Autonomous orbit determination systems use only measurements that are available on board a spacecraft. References 2-9 discuss various autonomous orbit determination schemes. The GPS system provides the possibility of a semi-autonomous system. A spacecraft can determine its orbit solely from the positions and velocities that it gets from its GPS receiver. This is not truly autonomous because the spacecraft relies on signals from the GPS system.

Different systems have widely different accuracy levels. Current ground-based systems can achieve position accuracies on the order of several centimeters[1]. GPS-based systems can have position accuracies ranging from about 100 m down to 0.1 meter, depending on whether or not differential GPS is being employed or the GPS signal has been intentionally degraded for non-U.S.-military users[2,10]. The truly autonomous systems advertise various levels of accuracy, ranging from 50 km down to 1 km or better. Many such systems have been studied only via simulation. Their true accuracies are not yet known.

The aims of the present work are to prove the observability of a new autonomous spacecraft orbit determination system and to estimate its likely accuracy. The new system can operate in Low Earth Orbit (LEO). It uses only a 3-axis magnetometer and a sun sensor, both on-board the spacecraft. In addition to estimating the spacecraft's orbit, the system also estimates the magnetometer's biases and corrections to a model of the Earth's magnetic field.

The proposed system is the latest in a sequence of systems that base their orbit determination capability on measurements of the Earth's magnetic field[4,6-9]. The original idea, as introduced by Psiaki *et al.*[4,6], was to compare on-board measurements of the Earth's magnetic field magnitude with a spherical harmonic model of that field. Any deviations were used to correct the orbit parameters. Using various filter designs, this basic system has been tested on flight data by Psiaki *et al.*[6], Shorshi and Bar-Itzhack[8], and Wiegand[9]. Achieved steady-state accuracies in these studies ranged from 8 km to 125 km. Accuracy was strongly influenced by the Earth field model's accuracy[6] and by field measurement accuracy[6,8,9]. Shorshi and Bar-Itzhack also tested a system that uses attitude data. It achieved accuracies on the order of 10-35 km when tested with real flight data[8].

Psiaki attacked the problem of inaccuracy in the Earth field model by developing a system that estimates corrections to this model while estimating the spacecraft orbit[7]. In order to make the orbit and field model coefficients simultaneously observable, this system included a 3-axis star sensor in addition to a 3-axis magnetometer. Simulation results predicted a system accuracy on the order of 300 m or better when using an accurate magnetometer and star sensor.

The present work is an extension of the work of Ref. 7. The new idea is to replace the 3-axis star sensor with a sun sensor. This would make the system much more economical. In fact, many missions already include a sun sensor and a magnetometer for attitude determination and control purposes. If the presently-

* Associate Professor, Sibley School of Mechanical and Aerospace Engineering. Associate Fellow, AIAA.

proposed system proved feasible, then it could be included on many missions at the cost of nothing more than some flops and memory in the flight computer.

There are 3 important questions in the present study. One is whether the spacecraft orbit and the magnetic field model coefficients remain simultaneously observable in a practical sense when only 2 axes worth of inertial attitude data are available; a sun sensor provides only 2-axes worth of data. If observability holds, then the other important questions are: What orbit/position accuracy might be achievable by such a system, and how does the achievable accuracy depend on orbit and system characteristics?

An added benefit of the proposed system may accrue to the attitude determination system. The Earth's magnetic field is typically not as accurate an attitude reference as the sun or the Earth limb. This is due to field model uncertainty. If the presently proposed system proves successful, then its magnetic field model corrections could be used to improve the magnetic attitude reference.

The present paper draws heavily on the methodology, models, and mathematics of Ref. 7. In order to conserve space, equations and models used in the present work normally will not be presented here if they can be found in that reference. Instead, the relevant equation number or section of that reference will be cited.

The remainder of this paper consists of 5 sections plus conclusions. Section 2 describes the batch filter that is used to estimate the orbit and the field model coefficients. This section describes the estimation vector, the orbital dynamics model, the measurement model, the least-squares technique used to solve the problem, and a statistical model of the filter's inputs and outputs. Section 3 describes covariance analysis and how it has been used to evaluate the proposed system. Section 4 describes a truth model and how it has been used to test the filter. Section 5 discusses the results of the analyses that are defined in Sections 3 and 4. Section 6 discusses computational practicalities such as execution speed and convergence robustness. Section 7 presents the conclusions.

II. Batch Filter Design

The Estimation Vector

The batch filter estimates a vector of quantities that define the spacecraft orbit and corrections to the Earth's magnetic field model. Exactly as in Ref. 7, that vector is defined to be

$$\mathbf{p} = \left[M_0, M_1, M_2, e, \omega_0, \lambda_0, i, b_x, b_y, b_z, q_1^0, q_1^1, s_1^1, \dot{q}_1^0, \dot{q}_1^1, \dot{s}_1^1, \dot{g}_1^0, \dot{g}_1^1, \dot{h}_1^1, \Delta g_1^0, \Delta g_1^1, \Delta h_1^1, \Delta g_2^0, \Delta g_2^1, \Delta h_2^1, \Delta g_2^2, \Delta h_2^2, \Delta g_3^0, \ldots, \Delta h_N^N \right]^T \quad (1)$$

These estimated quantities can be broken down into 3 main categories: the components that define the orbit, elements 1-7, the magnetometer biases, elements 8-10, and the corrections to the Earth's magnetic field, elements 11 and up.

The orbital and magnetometer bias estimation parameters are defined as follows: M_0, M_1, e, ω_0, λ_0, and i are standard Kepler elements. They are, respectively, the mean anomaly at epoch, the mean motion at epoch, the eccentricity, the argument of perigee at epoch, the longitude of the ascending node at epoch, and the inclination. M_2 $(= \dot{M}_1/2)$ is not a standard Kepler element; it constitutes an approximate way to model one of the main effects of drag. The magnetometer biases are b_x, b_y, and b_z, all measured in spacecraft-fixed coordinates.

The field correction elements in **p** are a) coefficients in a spherical harmonic expansion, b) time rates of change of coefficients, or c) perturbations of coefficients. The coefficients q_1^0, q_1^1, and s_1^1 are from a first-order external ring current model at epoch, and the corresponding rate terms, $\dot{q}_1^0$, $\dot{q}_1^1$, and $\dot{s}_1^1$, allow a constant time rate of change of the ring current, consistent with post-magnetic-storm field activity. The rate terms $\dot{g}_1^0$, $\dot{g}_1^1$, and $\dot{h}_1^1$ allow for an induced variation of the first-degree coefficients of the internal field, which is consistent with the normal effects of an external ring current. The rest of the **p** vector's elements, $\Delta g_1^0, \ldots, \Delta h_N^N$, are coefficient perturbations. They account for uncertainty in the main internal spherical harmonic field model at epoch as given by some standard field model such as the International Geomagnetic Reference Field (IGRF) for a particular half decade[11]. These perturbations go up to Nth-degree and Nth-order.

The length of the estimated **p** vector is $(19 + N^2 + 2N)$. If N = 10 is used for the magnetic field model perturbations, then **p** has 139 elements. Many of the cases considered in Section 5 correspond to this size **p** vector.

Model of Orbital Motion

The batch filter uses a physics-based model of the orbital dynamics. It gives the geocentric position time history as a function of the Kepler elements at epoch and a drag parameter. The model takes the form:

$$\theta = \theta(\Delta t; M_0, M_1, M_2, e, \omega_0, \lambda_0, i) \quad (2a)$$

$$\phi = \phi(\Delta t; M_0, M_1, M_2, e, \omega_0, \lambda_0, i) \quad (2b)$$

$$r = r(\Delta t; M_0, M_1, M_2, e, \omega_0, \lambda_0, i) \quad (2c)$$

where Δt = time since epoch, θ = colatitude, ϕ = longitude, and r = geocentric radius. This is the same model form as used in Ref. 7.

Models of varying degrees of fidelity can be formally represented by the form of eqs. (2a)-(2c). A high fidelity model would use a number of terms in the spherical harmonic expansion of Earth's gravity field, an accurate atmospheric model, and solar and lunar gravity perturbations, to mention a few of the effects. These added complexities can be important when filtering actual flight data, but they are not important to the question of whether the system at hand is observable in a practical sense. Therefore, a relatively simple orbital model has been used. It only includes gravity terms out to the J_2 term, and even then only the secular J_2 effects are included. The drag model only includes the effects on altitude and mean motion. This simplified model is given in the Appendix of Ref. 7.

Model of Sensor Measurements

The sensors available to the system are a 3-axis magnetometer and a 2-axis sun sensor. In the discussion that follows, suppose that the measured magnetic field vector at sample time Δt_k is $\mathbf{B}_{mes(k)}$ and that the measured sun direction unit vector at the same sample instant is $\hat{\mathbf{s}}_{mes(k)}$, with both expressed in spacecraft coordinates.

Two Pseudo Measurements and Their Statistics. The measurements have been manipulated to yield pseudo "measurements" that retain all of the position/orbit information of the original measurements but that are independent of spacecraft attitude. This independence allows decoupling of the attitude and orbit determination problems. The two useful pseudo measurements are the measured magnitude of the Earth's magnetic field and the measured cosine of the angle between the Earth's magnetic field vector and the sun direction vector. Their formulas in terms of the actual measurements are

$$y_{1mes(k)}(\mathbf{p}) = \sqrt{(\mathbf{B}_{mes(k)} - \mathbf{b})^T (\mathbf{B}_{mes(k)} - \mathbf{b})} \quad (3a)$$

$$y_{2mes(k)}(\mathbf{p}) = \frac{\hat{\mathbf{s}}_{mes(k)}^T (\mathbf{B}_{mes(k)} - \mathbf{b})}{y_{1mes(k)}(\mathbf{p})} \quad (3b)$$

where $\mathbf{b} = [b_x, b_y, b_z]^T$ is the estimated magnetometer bias vector in spacecraft coordinates. Its inclusion in these formulas is why the pseudo measurements depend on $\mathbf{p}$.

At times the sun vector measurement $\hat{\mathbf{s}}_{mes(k)}$ may be unavailable, either due to eclipse or due to a spacecraft attitude that takes the sun outside the sun sensor field of view. In either case pseudo measurement $y_{2mes(k)}$ will be unavailable.

Noise models for the pseudo measurements can be derived from the noise models for the actual measurements. Suppose that the noise models of the actual measurements are

$$\mathbf{B}_{mes(k)} = \mathbf{B}_{act(k)} + \mathbf{b} + \mathbf{n}_{B(k)} \quad (4a)$$

$$\hat{\mathbf{s}}_{mes(k)} = \hat{\mathbf{s}}_{act(k)} + \mathbf{n}_{s(k)} \quad (4b)$$

where $\mathbf{B}_{act(k)}$ is the actual magnetic field vector in spacecraft coordinates, $\hat{\mathbf{s}}_{act(k)}$ is the actual sun direction unit vector in spacecraft coordinates, and $\mathbf{n}_{B(k)}$ and $\mathbf{n}_{s(k)}$ are random, Gaussian, uncorrelated, discrete-time white noise measurement error vectors. All of these vectors correspond to sample time Δt_k. The statistics of the noise vectors are:

$$E\{\mathbf{n}_{B(k)}\} = 0, E\{\mathbf{n}_{B(j)}\mathbf{n}_{B(k)}^T\} = \mathbf{I}\,\sigma_B^2\,\delta_{jk} \quad (5a)$$

$$E\{\mathbf{n}_{s(k)}\} = 0, E\{\mathbf{n}_{s(j)}\mathbf{n}_{s(k)}^T\} = (\mathbf{I} - \hat{\mathbf{s}}_{act(k)}\hat{\mathbf{s}}_{act(k)}^T)\,\sigma_s^2\,\delta_{jk} \quad (5b)$$

$$E\{\mathbf{n}_{B(j)}\mathbf{n}_{s(k)}^T\} = \mathbf{0} \quad (5c)$$

The noise model for the pseudo measurements is derived using eqs. (3a)-(4b). First, one substitutes eqs. (4a) and (4b) into eqs. (3a) and (3b) and forms Taylor series expansions in terms of the noise vectors, $\mathbf{n}_{B(k)}$ and $\mathbf{n}_{s(k)}$. The resulting equations are:

$$y_{1mes(k)} = \sqrt{\mathbf{B}_{act(k)}^T \mathbf{B}_{act(k)}} + \frac{\mathbf{B}_{act(k)}^T \mathbf{n}_{B(k)}}{\sqrt{\mathbf{B}_{act(k)}^T \mathbf{B}_{act(k)}}} + O(\mathbf{n}_{B(k)}^2) \quad (6a)$$

$$y_{2mes(k)} = \frac{\hat{\mathbf{s}}_{act(k)}^T \mathbf{B}_{act(k)}}{\sqrt{\mathbf{B}_{act(k)}^T \mathbf{B}_{act(k)}}} + \frac{\mathbf{B}_{act(k)}^T \mathbf{n}_{s(k)}}{\sqrt{\mathbf{B}_{act(k)}^T \mathbf{B}_{act(k)}}} + \frac{\hat{\mathbf{s}}_{act(k)}^T}{\sqrt{\mathbf{B}_{act(k)}^T \mathbf{B}_{act(k)}}} \left[\mathbf{I} - \frac{\mathbf{B}_{act(k)}\mathbf{B}_{act(k)}^T}{\mathbf{B}_{act(k)}^T \mathbf{B}_{act(k)}}\right] \mathbf{n}_{B(k)} + O(\mathbf{n}_{s(k)}^2, \mathbf{n}_{s(k)}\mathbf{n}_{B(k)}, \mathbf{n}_{B(k)}^2) \quad (6b)$$

If one neglects the higher-order terms in $\mathbf{n}_{B(k)}$ and $\mathbf{n}_{s(k)}$, then these equations can be re-written in the form:

$$y_{1mes(k)} = y_{1act(k)} + n_{y1(k)} \quad (7a)$$

$$y_{2mes(k)} = y_{2act(k)} + n_{y2(k)} \quad (7b)$$

where $y_{1act(k)}$ is defined as the first term on the right-hand side of eq. (6a), $n_{y1(k)}$ is defined as the second term on the right-hand side of eq. (6a), $y_{2act(k)}$ is defined as the first term on the right-hand side of eq. (6b), and $n_{y2(k)}$ is defined as the sum of the second and third terms on the right-hand side of eq. (6b). These definitions of the error terms, coupled with the statistical models of $\mathbf{n}_{B(k)}$ and $\mathbf{n}_{s(k)}$ in eqs. (5a)-(5c), can be used to deduce the following statistical models for $n_{y1(k)}$ and $n_{y2(k)}$:

$$E\{n_{y1(k)}\} = 0, \qquad E\{n_{y1(j)}n_{y1(k)}\} = \sigma_B^2\,\delta_{jk} \quad (8a)$$

$E\{n_{y2(k)}\} = 0,$

$$E\{n_{y2(j)}n_{y2(k)}\} = \left(1-\frac{(\hat{\mathbf{s}}_{act(k)}^{T}\mathbf{B}_{act(k)})^2}{\mathbf{B}_{act(k)}^{T}\mathbf{B}_{act(k)}}\right)\bullet \left(\sigma_s^2+\frac{\sigma_B^2}{\mathbf{B}_{act(k)}^{T}\mathbf{B}_{act(k)}}\right)\delta_{jk} \quad (8b)$$

$$E\{n_{y1(j)}n_{y2(k)}{}^{T}\} = 0 \quad (8c)$$

Thus, the two pseudo measurements have errors that are statistically uncorrelated. Strictly speaking, these results are valid only in the limit of small measurement noise because linearizations were used to derive them.

It is helpful to redefine the variance for $n_{y2(k)}$ as

$$\{\sigma_{y2(k)}\}^2 = \left(1-\frac{(\hat{\mathbf{s}}_{mes(k)}^{T}\mathbf{B}_{mes(k)})^2}{\mathbf{B}_{mes(k)}^{T}\mathbf{B}_{mes(k)}}\right)\left(\sigma_s^2+\frac{\sigma_B^2}{\mathbf{B}_{mes(k)}^{T}\mathbf{B}_{mes(k)}}\right) \quad (9)$$

This differs slightly from eq. (8b), but the difference is not significant if the measurement errors and biases are relatively small. The variance definition in eq. (9) is preferable to the original one given in terms of $\mathbf{B}_{act(k)}$ and $\hat{\mathbf{s}}_{act(k)}$ because the latter quantities are never known exactly.

Models of the Pseudo Measurements. The filter needs a model of what the measurements should be for a given value of its estimated **p** vector.

The measurement model makes use of a spherical harmonic expansion of the Earth's magnetic field. The functional form of this spherical harmonic model is:

$$\mathbf{B}_{sez}(\theta,\phi,r;\mathbf{p},\Delta t) = \begin{bmatrix} B_\theta(\theta,\phi,r;\mathbf{p},\Delta t) \\ B_\phi(\theta,\phi,r;\mathbf{p},\Delta t) \\ B_r(\theta,\phi,r;\mathbf{p},\Delta t) \end{bmatrix} \quad (10)$$

where $\mathbf{B}_{sez}(\theta,\phi,r;\mathbf{p},\Delta t)$ is expressed in local south-east-zenith coordinates. The exact form of this model is given in eqs. (3a)-(3c) of Ref. 7. As denoted in eq. (10), the field depends on the geocentric position, (θ,ϕ,r), and on the field model coefficients and coefficient perturbations in the **p** estimation vector. $\mathbf{B}_{sez}$ depends directly on time because of the field model coefficient rate terms, $\dot{q}_1^0$, $\dot{q}_1^1$, $\dot{s}_1^1$, $\dot{g}_1^0$, $\dot{g}_1^1$, and $\dot{h}_1^1$.

The function $\mathbf{B}_{sez}(\theta,\phi,r;\mathbf{p},\Delta t)$ can be used to compute the modeled value of the first pseudo measurement as a function of the estimation vector and the sample time:

$$y_{1mod}(\Delta t_k;\mathbf{p}) = \{\mathbf{B}_{sez}^{T}[\theta(\Delta t_k,\mathbf{p}),\phi(\Delta t_k,\mathbf{p}),r(\Delta t_k,\mathbf{p});\mathbf{p},\Delta t_k]\bullet \mathbf{B}_{sez}[\theta(\Delta t_k,\mathbf{p}),\phi(\Delta t_k,\mathbf{p}),r(\Delta t_k,\mathbf{p});\mathbf{p},\Delta t_k]\}^{1/2} \quad (11)$$

The dependence of θ, ϕ, and r on Δt_k and **p** have been explicitly presented in this formula in order to completely express the dependence of y_{1mod} on these two quantities.

The model for y_2's dependence on Δt_k and **p** can be derived in the inertial celestial coordinate system, the system with +x in the equatorial plane and pointing towards the first point of Aries and with +z pointing along the north pole. The transformation from local south-east-zenith coordinates to celestial coordinates is $\mathbf{A}_{cc/sez}(\gamma_0,\theta,\phi,\Delta t)$, where γ_0 is the Greenwich hour angle at epoch. Given $\mathbf{A}_{cc/sez}$ and the sun unit vector in celestial coordinates at sample k, $\hat{\mathbf{s}}_{cc(k)}$, the model for the second pseudo measurement becomes:

$$y_{2mod}(\Delta t_k;\mathbf{p}) = \{\hat{\mathbf{s}}_{cc(k)}^{T}\,\mathbf{A}_{cc/sez}[\gamma_0,\theta(\Delta t_k,\mathbf{p}),\phi(\Delta t_k,\mathbf{p})]\bullet \mathbf{B}_{sez}[\theta(\Delta t_k,\mathbf{p}),\phi(\Delta t_k,\mathbf{p}),r(\Delta t_k,\mathbf{p});\mathbf{p},\Delta t_k]\}\bullet \{1/y_{1mod}(\Delta t_k,\mathbf{p})\} \quad (12)$$

Error Equations, Nonlinear Least Squares Estimator, and Statistical Interpretation

The goal of the batch filter is to choose the **p** estimation vector that best matches the pseudo measurements to their modeled values. Mathematically this leads to the following system of error equations:

$$e_{1(k)} = \frac{1}{\sigma_B}\{y_{1mod}(\Delta t_k;\mathbf{p}) - y_{1mes(k)}(\mathbf{p})\} \quad \text{for } k = 1, ..., N \quad (13a)$$

$$e_{2(k)} = \frac{1}{\sigma_{y2(k)}}\{y_{2mod}(\Delta t_k;\mathbf{p}) - y_{2mes(k)}(\mathbf{p})\} \quad \text{for all } k = 1, ..., N \text{ s.t. } \hat{\mathbf{s}}_{mes(k)} \text{ is available} \quad (13b)$$

where N is the number of samples in the batch. These equations have been scaled by the associated standard deviation in order to normalize the standard deviation of the errors $e_{1(k)}$ and $e_{2(k)}$.

The batch filter estimates **p** by computing the value that minimizes the sum of the square errors from eqs. (13a) and (13b). The estimate of **p** minimizes

$$J(\mathbf{p}) = \frac{1}{2}\sum_{k=1}^{N}\left[\frac{y_{1mod}(\Delta t_k;\mathbf{p}) - y_{1mes(k)}(\mathbf{p})}{\sigma_B}\right]^2 + \frac{1}{2}\sum_{k\,s.t.\,\hat{s}_{mes(k)}\,avail.}\left[\frac{y_{2mod}(\Delta t_k;\mathbf{p}) - y_{2mes(k)}(\mathbf{p})}{\sigma_{y2(k)}}\right]^2 \quad (14)$$

The filter solves this nonlinear least-squares problem using the iterative Gauss-Newton numerical

method. Reference 12 gives the details of this algorithm.

The partial derivatives of $y_{1mes}(\Delta t_k;\mathbf{p})$, $y_{2mes}(\Delta t_k;\mathbf{p})$, $y_{1mod}(\Delta t_k;\mathbf{p})$, and $y_{2mod}(\Delta t_k;\mathbf{p})$ with respect to $\mathbf{p}$ are needed. They are needed for observability analysis, to solve for search directions in the Gauss-Newton method, and to infer the error statistics of the $\mathbf{p}$ estimate. The needed partial derivatives are:

$$\frac{\partial y_{1mes(k)}}{\partial \mathbf{p}} = \frac{-(\mathbf{B}_{mes(k)} - \mathbf{b})^T \dfrac{\partial \mathbf{b}}{\partial \mathbf{p}}}{y_{1mes(k)}} \qquad (15a)$$

$$\frac{\partial y_{2mes(k)}}{\partial \mathbf{p}} = -\frac{\hat{\mathbf{s}}^T_{mes(k)} \dfrac{\partial \mathbf{b}}{\partial \mathbf{p}}}{y_{1mes(k)}} - \left[\frac{y_{2mes(k)}}{y_{1mes(k)}}\right]\frac{\partial y_{1mes(k)}}{\partial \mathbf{p}} \qquad (15b)$$

$$\frac{\partial y_{1mod(k)}}{\partial \mathbf{p}} = \frac{\mathbf{B}^T_{sez}\left\{\dfrac{\partial \mathbf{B}_{sez}}{\partial \theta}\dfrac{\partial \theta}{\partial \mathbf{p}} + \dfrac{\partial \mathbf{B}_{sez}}{\partial \phi}\dfrac{\partial \phi}{\partial \mathbf{p}} + \dfrac{\partial \mathbf{B}_{sez}}{\partial r}\dfrac{\partial r}{\partial \mathbf{p}} + \dfrac{\partial \mathbf{B}_{sez}}{\partial \mathbf{p}}\right\}}{y_{1mod(k)}} \qquad (15c)$$

$$\frac{\partial y_{2mod(k)}}{\partial \mathbf{p}} = \hat{\mathbf{s}}^T_{cc(k)}\left\{\left[\frac{\partial \mathbf{A}_{cc/sez}}{\partial \theta}\mathbf{B}_{sez} + \mathbf{A}_{cc/sez}\frac{\partial \mathbf{B}_{sez}}{\partial \theta}\right]\frac{\partial \theta}{\partial \mathbf{p}} + \left[\frac{\partial \mathbf{A}_{cc/sez}}{\partial \phi}\mathbf{B}_{sez} + \mathbf{A}_{cc/sez}\frac{\partial \mathbf{B}_{sez}}{\partial \phi}\right]\frac{\partial \phi}{\partial \mathbf{p}} + \mathbf{A}_{cc/sez}\left[\frac{\partial \mathbf{B}_{sez}}{\partial r}\frac{\partial r}{\partial \mathbf{p}} + \frac{\partial \mathbf{B}_{sez}}{\partial \mathbf{p}}\right]\right\}/y_{1mod(k)} - \left[\frac{y_{2mod(k)}}{y_{1mod(k)}}\right]\frac{\partial y_{1mod(k)}}{\partial \mathbf{p}} \qquad (15d)$$

Linearized versions of eqs. (13a) and (13b) can be used to infer the statistics of the error in the estimate of $\mathbf{p}$. The linearized equations take the form

$$\begin{bmatrix} e_{1(1)} \\ \vdots \\ e_{1(N)} \\ e_{2(1)} \\ \vdots \\ e_{2(N)} \end{bmatrix} = \mathbf{A}\,\Delta\mathbf{p} \qquad (16a)$$

with

$$\mathbf{A} = \begin{bmatrix} \dfrac{1}{\sigma_B}\left\{\dfrac{\partial y_{1mod(1)}}{\partial \mathbf{p}} - \dfrac{\partial y_{1mes(1)}}{\partial \mathbf{p}}\right\} \\ \vdots \\ \dfrac{1}{\sigma_B}\left\{\dfrac{\partial y_{1mod(N)}}{\partial \mathbf{p}} - \dfrac{\partial y_{1mes(N)}}{\partial \mathbf{p}}\right\} \\ \dfrac{1}{\sigma_{y2(1)}}\left\{\dfrac{\partial y_{2mod(1)}}{\partial \mathbf{p}} - \dfrac{\partial y_{2mes(1)}}{\partial \mathbf{p}}\right\} \\ \vdots \\ \dfrac{1}{\sigma_{y2(N)}}\left\{\dfrac{\partial y_{2mod(N)}}{\partial \mathbf{p}} - \dfrac{\partial y_{2mes(N)}}{\partial \mathbf{p}}\right\} \end{bmatrix} \qquad (16b)$$

where $\mathbf{A}$ is the Jacobian matrix of eqs. (13a) and (13b) and where the y_2 rows are omitted for sample times that lack sun sensor data. If $\mathbf{p}_{act}$ is the true value of $\mathbf{p}$ and if $\hat{\mathbf{p}}$ is the estimated value from the filter's nonlinear least-squares solver, then the linearized estimate of the error covariance is:

$$\mathbf{P}_p = E\{(\mathbf{p}_{act} - \hat{\mathbf{p}})(\mathbf{p}_{act} - \hat{\mathbf{p}})^T\} = (\mathbf{A}^T\mathbf{A})^{-1} \qquad (17)$$

III. Covariance Analysis and Practical Observability

The system is theoretically observable in the linearized sense if the Jacobian matrix $\mathbf{A}$ has full column rank. This is true because the observability Gramian of the linearized system is $\mathbf{A}^T\mathbf{A}$.

Practical observability depends on the distance of $\mathbf{A}^T\mathbf{A}$ away from singularity. Distance is a relative notion that changes with problem scaling. Therefore, a better measure of observability is the covariance of the estimated vector, $\mathbf{P}_p = (\mathbf{A}^T\mathbf{A})^{-1}$. If all of the standard deviations, the square roots of the diagonals of $\mathbf{P}_p$, are small in a problem-dependent sense, then the system is practically observable because these quantities' smallness implies that $\mathbf{A}^T\mathbf{A}$ is nonsingular, which implies that the system is observable.

The standard deviations of the magnetometer biases and of the magnetic field model corrections will be used as practical measures of these quantities' observability.

Actual spacecraft position standard deviations are better measures of practical observability than are the standard deviations of the Kepler elements and the drag term. The spacecraft's instantaneous position variance can be inferred from $\mathbf{P}_p$, in a linearized sense, via application of the chain rule and of the definition of covariance. Equations (11) and (12) of Ref. 7 give a method for inferring the along-track/cross-track/altitude covariance matrix at a particular time as a function of $\mathbf{P}_p$ and $\hat{\mathbf{p}}$. Three good measures of practical orbit observability are the maxima, taken over the batch time interval, of the standard deviations of the three position error components.

IV. Testing Against a Simulated Truth Model

Comparison of Filter Outputs with Truth Model Values.

The proposed system has been studied using simulated data from a truth model. The truth model contains dynamics, measurements, and noise. It produces simulated magnetometer and sun sensor data. The simulated output data is fed into the filter, which produces an estimate of the truth model's orbit and field.

Filter performance can be evaluated by comparing the truth model's orbit and field to the filter's estimate of these quantities. Comparison of individual cases reveals the amount of error that is caused by systematic (i.e., non-statistical) effects.

Several types of comparisons are made between truth model values and the filter output. The estimated orbit is compared with the truth model orbit in terms of along-track, cross-track, and altitude error. The magnetometer biases and the field model coefficient perturbations are compared. The inertial direction of the estimated magnetic field at the estimated spacecraft location is compared with the inertial direction of the truth-model magnetic field at the truth-model spacecraft location.

Truth Models of Orbit and Attitude Dynamics

The truth model of the orbital dynamics uses the same model as is used in the filter because the effect of filter dynamic model fidelity is not considered to be the critical issue. The truth model uses the truth values of the Kepler elements M_0, M_1, e, ω_0, γ_0, and i and the truth value of the drag parameter M_2. These are elements of the $\mathbf{p}_{truth}$ vector. These values are input to eqs. (2a)-(2c) to generate the truth-model spacecraft position time history.

The spacecraft's attitude dynamics might affect the observability of the system or the accuracy of the filter. This comes about because the estimated magnetometer biases are defined along spacecraft body axes and because the attitude time history might take the sun outside of the sun sensor's limited field of view.

Two different types of attitude time history have been used in the truth model. One is for a nadir-pointing spacecraft. The other is for a spin-stabilized spacecraft. Both attitude dynamics models produce a transformation from celestial coordinates to spacecraft coordinates, $\mathbf{A}_{sc/cc}(\Delta t)$, that is a function of time.

Truth Models of Measurements

Each truth-model magnetometer measurement is constructed by a multi-step process. First, the truth model spacecraft position coordinates, θ_k, ϕ_k, and r_k, are computed for sample time Δt_k using $\mathbf{p}_{truth}$ and eqs. (2a)-(2c). Next, these position components, Δt_k, and $\mathbf{p}_{truth}$ are used in eq. (10) to determine the truth value of the field in south-east-zenith coordinates, $\mathbf{B}_{sez(k)}$. Third, θ_k, ϕ_k, the Greenwich hour angle at epoch, γ_0, and Δt_k, are used to compute the truth-value transformation from local south-east-zenith coordinates to celestial coordinates, $\mathbf{A}_{cc/sez(k)}$. Next, $\mathbf{A}_{cc/sez(k)}$ is used with the truth-model attitude transformation, $\mathbf{A}_{sc/cc(k)}$, to transform $\mathbf{B}_{sez(k)}$ into spacecraft coordinates: $\mathbf{B}_{sc(k)} = \mathbf{A}_{sc/cc(k)}\mathbf{A}_{cc/sez(k)}\mathbf{B}_{sez(k)}$. Finally, the truth value of the magnetometer bias vector and a random noise vector are added in to yield the truth-model magnetometer measurement vector: $\mathbf{B}_{mes(k)} = \mathbf{B}_{sc(k)} + \mathbf{b}_{truth} + \mathbf{n}_{B(k)}$.

There are two types of errors between the truth model magnetic field and the filter's initial guess of the Earth's magnetic field. First, $\mathbf{B}_{sez}$ is affected by the truth values of the field model coefficient perturbations contained in $\mathbf{p}_{truth}$. In addition, the truth magnetic field model may contain terms beyond those of the filter. For many cases considered in the present study, the filter used a 10th-degree, 10th-order field model, but the truth model used a 13th-degree, 13th-order model. This addition of higher-order terms to the spherical harmonic model of the field constitutes a systematic error between the truth model and the filter.

The truth model of the sun sensor measurements includes noise and considers eclipse by the Earth and the finite width of the sun sensor field of view. The visibility of the sun is determined from the spacecraft position and the sun unit vector. If not in eclipse, then the sun measurement vector is computed by using the truth model spacecraft attitude to calculate $\hat{\mathbf{s}}_{sc(k)} = \mathbf{A}_{sc/cc(k)}\,\hat{\mathbf{s}}_{cc(k)}$ and a random noise vector to determine $\hat{\mathbf{s}}_{mes(k)} = (\hat{\mathbf{s}}_{sc(k)} + \mathbf{n}_{s(k)})/\|\hat{\mathbf{s}}_{sc(k)} + \mathbf{n}_{s(k)}\|$. The statistics of $\mathbf{n}_{s(k)}$ are defined by eq. (5b). Given $\hat{\mathbf{s}}_{mes(k)}$, the truth model verifies that it falls within the field of view of the sun sensor, which is defined in spacecraft coordinates, before recording it as a measurement.

V. Results

Covariance-Based Practical Observability of Various Cases

The system has proved observable in many important cases. It is theoretically observable in all situations except that of an orbit with zero inclination and zero eccentricity. That is, its $\mathbf{A}^T\mathbf{A}$ Gramian matrix is nonsingular in those cases. It is practically observable in most situations that are sufficiently far away from having zero inclination and zero eccentricity.

The dependence of estimation standard deviations on orbit parameters has been extensively investigated. A sequence of cases have been considered that all respect the following set of assumptions: The filter estimates coefficient corrections for a 10th-degree, 10th-order field model. The spacecraft is spinning with a spin period of 50.235 sec., and its spin axis is sun-pointed. The magnetometer accuracy is 10 nT 1-σ for the random white noise component -- the biases can be much larger because they get estimated. The sun sensor accuracy is 0.005 deg. 1-σ, and this error source is primarily random white noise. The inter-sample interval is $\Delta t_k - \Delta t_{k-1} = 60$ sec., and the total number of samples is N = 1441; this means that each batch contains one full day's worth of data. The relationship between the sun direction and the orbit is such that eclipse occurs for as much as 37% of the orbit for some inclinations and orbital altitudes.

Estimation standard deviations for these cases are given as functions of orbital parameters in Table 1. The 2nd through 4th columns of the table give the orbital characteristics for the case: inclination, apogee height, and perigee height. The next 3 columns give the maximum position standard deviations during the batch interval, where "A-T" stands for along-track and "C-T" stands for cross-track. The 8th column gives the maximum standard deviation for the three 1st-degree field coefficient corrections, Δg_1^0, Δg_1^1, and Δh_1^1. The last column gives the maximum standard deviation of the 3 magnetometer biases, b_x, b_y, and b_z.

Table 1 demonstrates the effect of inclination, eccentricity, and altitude on observability. Practical observability decreases with inclination as evidenced in Cases 1-5. All 5 of the tabulated standard deviations increase as inclination decreases. Observability decreases with increased altitude, as evidenced by Cases 2 and 7. Eccentricity helps observability. Otherwise, the standard deviations of case 8, which has a very low inclination but significant eccentricity, would have been much higher.

These results are similar to what was found in Ref. 7, where data from a 3-axis star sensor was made available to the filter. One would expect the results in Ref. 7 to be at least as good as the present results. This is generally the case, but Ref. 7's results are better only by a factor of about 2 or less. The present results are remarkable because they derive from one axis less of attitude data and from attitude data that is less accurate by a factor of 9.

As an illustration of the type of result that the covariance analysis produces, Fig. 1 presents 3 position error component standard deviations as functions of time. These correspond to Case 2 in Table 1. Recall that these standard deviations are inferred by propagating the covariances of the Kepler elements through various (linearized) geometric transformations. The data in Table 1 are the maximum values of each of these three curves over the interval. One can see that the along-track standard deviation has a secular component. This is the result of uncertainty in the estimated orbital period and drag term.

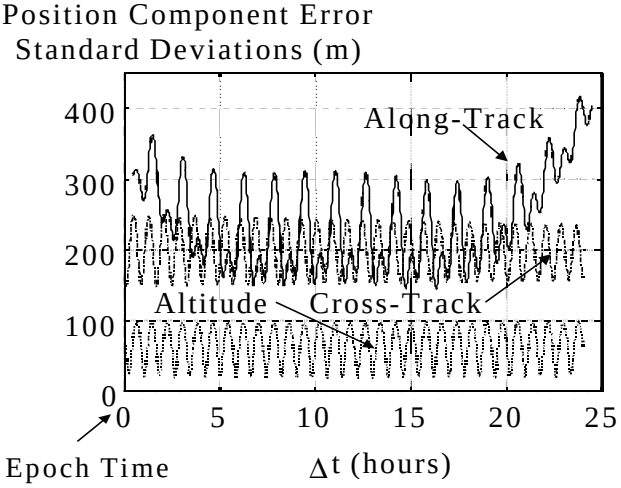

Fig. 1 Position error component standard deviations versus time for a representative case.

Figure 2 presents the standard deviations of the field perturbation elements of a **p** estimation vector. This particular set of data corresponds to Case 2 of Table 1. These perturbations are element numbers 11 through $(2N + N^2 + 19)$ of **p**. The standard deviations are plotted versus the element number. The secular rate perturbation coefficients have been multiplied by the batch duration, $(\Delta t_N - \Delta t_1)$ before being plotted; this gives their effects in nT at the end of the interval. As can be seen, this filter's ability to estimate field perturbations degrades for higher spherical harmonic degrees. This is different from the results of Ref. 7. In that study, if inclination and eccentricity were not too close to zero, then the field model coefficients could be estimated accurately for all degrees and orders in the model.

The effect of the availability of the sun has been investigated. A case has been run that is like Case 2 in Table 1 except that the sun is never in eclipse behind the Earth. For this case the 3 maximum standard deviations of the position error components are: 781m along-track, 138m across-track, and 158m in altitude. This is surprising. Intuition suggests that the availability of more data should increase accuracy, but along-track and altitude accuracy actually decrease. Presumably, this is an effect of the change in geometry

between the orbit normal vector and the sun observation vector.

Another variable that is related to sun availability is the type of attitude dynamics that the spacecraft has. A nadir-pointing spacecraft with a limited sun sensor field of view will collect less sun direction data than a properly designed sun-pointing spin-stabilized spacecraft. This study considered a nadir-pointing spacecraft model with a 128^o-diameter sun sensor field of view. It consistently achieved poorer position error standard deviations than the spin-stabilized, sun-pointing spacecraft. For the nadir-pointing spacecraft in an orbit like that of Case 2 in Table 1, the filter's maximum position standard deviations are: 908m along-track, 319m across-track, and 352m in altitude, which is obviously worse than the sun-pointing case that is given in the table. This comparison typifies many other cases.

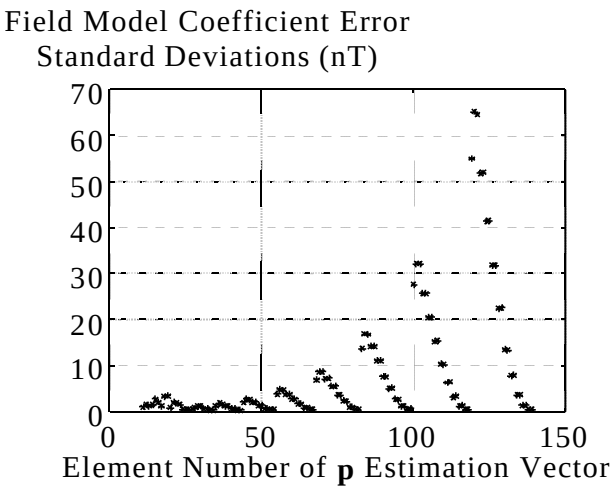

Fig. 2 Field model coefficient standard deviations for a representative case.

The sensors' accuracies have a direct impact on the filter's predicted standard deviations. It is obvious that more accurate sensors would yield lower predicted errors, but the relative effects of the two sensors' variances is less obvious. A series of cases have been run that are like Case 2 of Table 1 except that the sun sensor accuracy, σ_s, has been varied. The results are given in Table 2. This table shows that the nominal sun sensor accuracy of $\sigma_s = 0.005^o$ is well matched with these cases' magnetometer accuracy, $\sigma_B = 10$nT. More sun sensor accuracy yields very little position accuracy improvement, but less sun sensor accuracy degrades the filter's performance.

The length of the filtering interval affects the position accuracy. A case has been run that is like Case 1 of Table 1 except that the time between samples has been lengthened from 60 sec to 120 sec. This means that 2 days' worth of data are used instead of 1 day's worth. The maximum position standard deviations for this case are: 262m along-track, 204m across-track, and 86m in altitude. This represents a 31% reduction in the peak along-track standard deviation. The other two standard deviations are reduced only modestly. This along-track accuracy improvement can be traced to increased accuracy of the estimates of the Kepler elements M_0 and M_1 and drag-like parameter M_2.

In order to illustrate the usefulness of the proposed system, a typical spacecraft case has been run. This case was designed to correspond to the ALEXIS spacecraft mission as much as possible[13]. The nominal ALEXIS orbit has an apogee of 830 km, a perigee of 740 km, and an inclination of 70^o. The ALEXIS fine sun sensor has an advertised accuracy of 0.05^o. A magnetometer accuracy of 10 nT was assumed for this case to increase the likelihood of achieving good results. ALEXIS is a spin-stabilized spacecraft whose spin axis points (roughly) towards the sun. The batch filter used one day's worth of data sampled at 60 sec. intervals, as in most other cases considered here. The maximum position standard deviations predicted for this case are: 899m along-track, 570m across-track, and 224m in altitude. These standard deviations place the 3σ position accuracy well within the 5 km spec. that was set for orbit knowledge on this mission.

Comparisons with Truth Model Outputs.

Various issues have been investigated by filtering data from the truth model and comparing the filter's estimated **p** vector with the truth value of **p**. Although true Monte Carlo analysis has not been done, truth model comparisons have been used to verify, in an approximate manner, the results of the covariance analysis. In all cases where only random errors were present, the highest ratio of an actual error to a pre-computed standard deviation was 2.48. Thus, the 3-σ rule, when applied using the predicted standard deviations from the covariance analysis, proved sufficient to bound the worst-case errors.

The effect of truncation of the field model has been investigated by truth-model/filter comparison. Four different filters have been considered, all operating on data from a simulated orbit like that of Case 2 in Table 1. Each uses a 10th-degree, 10th-order model of the Earth's magnetic field, but each estimates corrections for a different number of the coefficients in its field model. One estimates corrections only up to the 7th degree and 7th order, another up to 8th degree and order, a third up 9th degree and order, and the fourth estimates corrections for all of the coefficients up to 10th degree and 10th order. The truth model's field was a 13th-degree/13th-order spherical harmonic

model. Thus, it differed from each of the filters' models for the 11th through 13th degree and order terms. For the lower-order terms, the truth model had random errors between its coefficients and the filters' *a priori* coefficients. These random errors had a normal distribution and a standard deviation of 1% of the nominal coefficient value. The filters were not given a model of these error sources. Random magnetometer and sun sensor errors were included, but their standard deviations, $\sigma_B = 0.1$ nT and $\sigma_s = 5 \times 10^{-5}$ deg, were small enough to make their effects negligible.

The number of missing correction terms in the field model truncation did not affect the results very significantly. For example, the maximum along-track errors between the filters' estimated orbits and the truth-model orbits were 328m, 381m, 378m, and 319m for the 4 respective filters, i.e., for the 7th, 8th, 9th, and 10th degree and order filters. The results are similar for the other position error components' peak values. Thus, the filter's position error is not degraded seriously if field model corrections are estimated only up to 7th degree and 7th order.

This result is consistent with Fig. 2, which shows that the filter does a poorer job of estimating higher-degree and higher-order field model coefficient corrections. It stands to reason that, if the filter cannot estimate a quantity very accurately, then it will do about as well if it uses an *a priori* estimate for that quantity. A reduction to 7th-degree and 7th-order corrections greatly reduces the number of elements in the **p** estimation vector, from 139 to 82. This reduction speeds computer execution times and reduces memory requirements.

There is a possible side benefit to simultaneous orbit and magnetic field model estimation. This benefit is an improvement of the modeled inertial direction of the Earth's magnetic field. Using currently available models of the Earth's magnetic field, the field model's local inertial direction may be wrong by as much as 0.4^o or more, assuming a 300 nT field error and a 40,000 nT field strength. In each of the comparisons with the truth model, the estimated and truth-model inertial directions of the Earth's magnetic field have been compared. The results are very encouraging. For simulations corresponding to the cases listed in Table 1 and with a 13th-degree/13-order truth field model, the maximum inertial direction error of the estimated field was 0.11^o. If Cases 5 and 8 had been eliminated because of their poorer general observability due to low inclination, then the maximum inertial direction error of the field would have been just 0.08^o.

This field direction accuracy opens up the possibility of changing standard attitude determination systems. These improved field model accuracies are comparable to those of standard Earth limb detectors[13]. It might be possible to fly a spacecraft with only a magnetometer and a sun sensor. These 2 sensors could be used to estimate both orbit and attitude. The attitude estimate could be accurate to better than 0.1^o on all three axes.

Comparisons with Simplified Filters.

Comparisons with simpler filters have been carried out in order to determine how the current filter achieves improvements. In comparison to the filter in Ref. 6, the current filter adds 2 features: the inclusion of sun sensor data and the estimation of field model coefficient corrections. Reference 8 found that inclusion of attitude data alone can improve the estimated position accuracy. Therefore, there is a question about the current filter: how much of its accuracy improvement comes from adding sun sensor data and how much comes from estimating field model coefficients?

This question has been answered by filtering truth-model data using 2 simplified filters. One filter was the same as described above, except that it did not estimate any field model coefficient perturbations. In this case the length of the **p** estimation vector was only 10. In the second case, the filter was further simplified by discarding the sun sensor measurements so that the y_2 pseudo measurement was not used. This latter filter was equivalent to the batch filter of Ref. 6. In both of these cases the truth model had a 13th-degree/13th-order field, and the filter used a 10th-degree/10th-order field. Where applicable, the filter's field model coefficients were set to be different than the corresponding coefficients of the truth model. These differences were random and normally distributed and had standard deviations equal to 1% of the nominal coefficients' magnitudes. To account for the increased uncertainty in the Earth's field, the value of σ_B was increased to 200 nT in both filters. The cases that were run corresponded to the orbital conditions of Case 1 in Table 1.

Both simplified filters showed significantly poorer performance than the filter that has been developed in this paper. The first filter, the one that used sun sensor data without estimating field model corrections, had the following peak position errors: 7,600 m along-track, 2,300 m across-track, and 1,100 m in altitude. The filter that used only magnetometer measurements did even worse. Its peak position errors were: 13,100 m along-track, 14,800 m across-track, and 800 m in altitude.

These results show that the addition of attitude data reduces the total position error by a factor of about 2. The attitude data produces its largest improvement in the determination of the orbital plane, which yields better cross-track accuracy. This is roughly the same as what was found in Ref. 8 for the GRO spacecraft.

These results show that it is important to add field model coefficient corrections to the filter's estimation vector. To see this, compare the results for Case 1 of Table 1 with the above results that use sun sensor measurements but no estimation of field model corrections. Suppose that Table 1's predicted maximum errors are 3 times the standard deviations listed in the table; i.e., assume 3σ limits. Then, for the simulation case considered in this section, the elimination of field coefficient corrections increased the maximum position component errors by factors ranging from 3.7 to 6.7, and the total position error was increased by a factor of about 6.7.

VI. Computational Issues

The issues of computer memory requirements, required computation time, and convergence robustness are important to consider as gauges of the proposed filter's practicality. All experience reported here is for runs on a 100 MHz Pentium using FORTRAN.

The memory requirements depend on the size of the **p** estimation vector. The filter's executable program and data storage occupied the following amounts of memory: 544 kbytes for 10th-degree/10th-order field model corrections, 475 kbytes for 9th-degree/9th-order corrections, 419 kbytes for 8th-degree/8th-order corrections, and 374 kbytes for 7th-degree/7th-order corrections.

The solution speed depends on the dimension of the **p** estimation vector and on the accuracy of the first guess. It makes the most sense to talk about the execution time per major Gauss-Newton iteration. The problem would be solvable in just one such iteration if it were linear. Multiple iterations are required to minimize the nonlinear least squares cost function. The computation time per iteration was 56 sec. per iteration for the filter with 10th-degree/10th-order field model corrections, 37 sec. for the filter with 9th-degree/9th-order corrections, 27 sec. for the 8th-degree/8th-order filter, and 21 sec. for the 7th-degree/7th-order filter.

The number of Gauss-Newton iterations required to solve for the estimate from a given set of data depended on the goodness of the initial guesses of the orbit, the magnetometer biases, and the field model. Typical runs had initial root mean square (rms) total position errors in the range 160-310 km and converged in 3 to 13 Gauss-Newton iterations. The worst initial position error for which successful convergence was achieved was 1420 km rms. This case took 9 Gauss-Newton iterations to converge. One case with an rms initial position error of 560 km took 20 Gauss-Newton iterations to converge.

Convergence robustness has been demonstrated by the ability to converge from 1400 km rms initial position error. Computational experience indicates that convergence from larger initial errors probably is feasible if the orbit parameterization is changed from Keplerian elements to something that does not have singularities.

VII. Conclusions

A batch filter has been designed to estimate the orbit of a LEO spacecraft, and its performance has been analyzed. The only sensor data that this filter needs are the measurements from a 3-axis magnetometer and from a sun sensor. The filter also estimates the magnetometer's biases and corrections to a spherical harmonic model of the Earth's magnetic field.

The position accuracy that the filter can achieve is sufficient for many real spacecraft missions. $3\text{-}\sigma$ accuracies on the order of 1,700 m or smaller are achievable for LEO orbits with inclinations of 45^o or more. These position accuracies depend on a number of factors. The sensor accuracies directly influence the result; the above results assume a per-axis $1\text{-}\sigma$ magnetometer accuracy of 10 nT excluding biases and a $1\text{-}\sigma$ sun sensor accuracy of 0.005^o. Geometric observability effects degrade the estimated position accuracy for inclinations below 45^o and as altitude increases.

A side benefit of the proposed system is increased accuracy of magnetometer-based attitude determination. The estimated corrections of the Earth's magnetic field model reduce the uncertainty in the inertial magnetic field direction to 0.1^o or less.

The proposed filter creates the possibility of a relatively inexpensive and effective combined attitude and orbit determination system. The only sensors would be a sun sensor and a magnetometer. The proposed system would be able to determine position to within 1.7 km and attitude to within 0.1^o.

References

1. Tapley, B.D., *et al*., "Precision Orbit Determination for TOPEX/POSEIDON," **Journal of Geophysical Research**, Vol. 99, No. C12, pp. 24,383-24,404, Dec. 1994.
2. Chory, M.A., Hoffman, D.D., and LeMay, J.L., "Satellite Autonomous Navigation -- Status and

History," **Proceedings of the IEEE Position, Location, and Navigation Symposium**, Las Vegas, NV, Nov. 4-7, 1986, pp. 110-121.

3. Tai, F. and Noerdlinger, P.D., "A Low Cost Autonomous Navigation System", AAS Paper 89-001, **Guidance and Control 1989**; **Proceedings of the Annual Rocky Mountain Guidance and Control Conf.**, Feb. 1989, Keystone, Colorado, pp. 3-23.
4. Psiaki, M.L. and Martel, F., "Autonomous Magnetic Navigation for Earth Orbiting Spacecraft", **Proceedings of the 3rd Annual AIAA/USU Conf. on Small Satellites**, Sept. 1989, Logan, Utah, pp. unnumbered.
5. Hicks, K.D. and Wiesel, W.E. Jr., "Autonomous Orbit Determination System for Earth Satellites," **Journal of Guidance, Control, and Dynamics**, Vol. 15, No. 3, May-June 1992, pp. 562-566.
6. Psiaki M.L., Huang L., and Fox S.M., "Ground Tests of Magnetometer-Based Autonomous Navigation (MAGNAV) for Low-Earth-Orbiting Spacecraft", **Journal of Guidance, Control, and Dynamics**, Vol. 16, No. 1, Jan.-Feb. 1993, pp. 206-214.
7. Psiaki M.L., "Autonomous Orbit and Magnetic Field Determination Using Magnetometer and Star Sensor Data", **Journal of Guidance, Control, and Dynamics**, Vol. 18, No. 3, May-June 1995, pp. 584-592.
8. Shorshi, G. and Bar-Itzhack, I.Y., "Satellite Autonomous Navigation Based on Magnetic Field Measurements", **Journal of Guidance, Control, and Dynamics**, Vol. 18, No. 4, July-Aug. 1995, pp. 843-850.
9. Wiegand, M., "Autonomous Satellite Navigation via Kalman Filtering of Magnetometer Data," **Acta Astronautica**, Vol. 38, 1996, pp. 395-403.
10. Wu, S.C., Yunck, T.P., and Thornton, C.L., "Reduced-Dynamic Technique for Precise Orbit Determination of Low Earth Satellites," **Journal of Guidance, Control, and Dynamics**, Vol. 14, No. 1, Jan.-Feb. 1991, pp. 24-30.
11. Langel, R.A., "The Main Field", in **Geomagnetism**, Jacobs, J.A., ed., Vol. 1, Academic Press, (New York, 1987), pp. 249-512.
12. Gill, P.E., Murray, W., and Wright, M.H., **Practical Optimization**, Academic Press, (New York, 1981).
13. Psiaki, M.L., Theiler, J., Bloch, J., Ryan, S., Dill, R.W., and Warner, R.E. “ALEXIS Spacecraft Attitude Reconstruction with Thermal/Flexible Motions Due to Launch Damage”, **Journal of Guidance, Control, and Dynamics**, Vol. 20, No. 5, Sept.-Oct. 1997, pp. 1033-1041.

Table 1
Orbit, Field Coefficient, and Bias Standard Deviations as Functions of Orbital Parameters

Case	i (deg)	Apogee Altitude (km)	Perigee Altitude (km)	Max. Component σ's A-T (m)	C-T (m)	Altitude (m)	Max. σ of 1st-deg. field (nT)	Max. σ of magnet. bias (nT)
1	88.1	585	515	379	206	90	1.9	0.7
2	75.0	585	515	415	250	98	2.0	0.7
3	45.0	585	515	560	381	116	6.3	1.2
4	30.0	585	515	761	579	149	38.4	1.7
5	15.0	585	515	1,326	1,160	216	1.29×10^3	2.1
6	75.0	3,200	500	607	616	178	2.9	0.7
7	75.0	3,200	3,100	1,531	1,214	405	6.6	0.9
8	1.0	3,200	500	4,410	3,724	531	1.43×10^4	1.0

Table 2
Orbit, Field Coefficient, and Bias Standard Deviations as Functions of Sun Sensor Accuracy

Case	σ_s	Max. Component σ's			Max. σ of	Max. σ of
		A-T	C-T	Altitude	1st-deg. field	magnet. bias
	(deg)	(m)	(m)	(m)	(nT)	(nT)
1	0.0005	404	244	97	2.0	0.7
2	0.005	415	250	98	2.0	0.7
3	0.05	795	498	198	3.9	1.1
4	0.25	1,396	2,104	404	8.8	1.6